Zhao, O., Gardner, L., & Young, B. (2016). Experimental Study of Ferritic Stainless Steel Tubular Beam-Column Members Subjected to Unequal End Moments. Journal of Structural Engineering (ASCE), 04016091.

Experimental study of ferritic stainless steel tubular beam-column members subjected to unequal end moments

Ou Zhao [1]; Leroy Gardner [2]; and Ben Young, M.ASCE [3]

Abstract: This paper presents a comprehensive experimental study of the buckling behavior of ferritic stainless steel tubular section beam-column structural members subjected to unequal end moments. Testing was carried out on two cold-formed and seam-welded cross-sections – one rectangular hollow section (RHS) 100×40×2 and one square hollow section (SHS) 60×60×3 made of grade AISI 410 (EN 1.4003) stainless steel. The experimental investigation included a series of material tensile coupon tests, initial local and global geometric imperfection measurements and twenty-four beam-column tests under unequal end moments. The experimental setup and procedures are described, and the test observations, including the key test results, the load–deformation histories and the failure modes, are fully reported. The experimental results were carefully analyzed and then compared with the design strength predictions determined according to the current European code, American specification and Australian/New Zealand standard for stainless steel structures, enabling the accuracy of each codified method to be evaluated. Generally, the European code resulted in the most conservative and scattered strength predictions among the three codified approaches, owing principally to the use of the same treatment for stainless steel beam-columns under both equal and unequal end moments. The American specification and Australian/New

[1] PhD Candidate, Dept. of Civil and Environmental Engineering, Imperial College London, London SW7 2AZ, UK. (Corresponding author). Email: ou.zhao11@imperial.ac.uk

[2] Professor of Structural Engineering, Dept. of Civil and Environmental Engineering, Imperial College London, London SW7 2AZ, UK. Email: leroy.gardner@imperial.ac.uk

[3] Professor of Structural Engineering, Dept. of Civil Engineering, The University of Hong Kong, Pokfulam Road, Hong Kong, China. Email: young@hku.hk

Zealand standard employ an equivalent uniform moment factor to consider the beneficial effects of moment gradient on beam-column strengths. These approaches were shown to offer more accurate and consistent capacity predictions for ferritic stainless steel beam-columns under unequal end moments, though further improvements remain possible.

Keywords: Beam-columns; Cold-formed; Design standards; Equivalent moment factor; Experiments; Ferritic stainless steel; Structural design; Unequal end moments;

1. Introduction

The aesthetic appeal, favorable mechanical properties and good ductility, coupled with the excellent corrosion resistance and minimal maintenance requirements, make cold-formed stainless steel structural members an increasingly attractive choice in a variety of engineering applications (Gardner 2008a). Given the high initial material cost of stainless steels, appropriate grade selection and structural design efficiency are primary concerns. For the design of stainless steel elements under combined loading, although a number of established structural design codes exist, the provisions were generally developed based on the corresponding carbon steel design rules, which often fail to reflect accurately the true structural response of stainless steel members. This has prompted research aimed at investigating the structural performance of stainless steel members under combined loading, assessing the accuracy of the existing design provisions and devising more refined design methods. A brief review of previously studies in this area is given below. At the cross-sectional level, a series of experimental and numerical studies on eccentrically-loaded SHS and RHS (Zhao et al. 2015a, b, c; Arrayago and Real 2015) and circular hollow section (CHS) (Zhao et al. 2016a, b) stub columns has been carried out to systematically investigate the local buckling behavior of stainless steel profiles under combined loading. The studies have highlighted undue conservatism in the existing stainless steel design codes, which results mainly from the neglect of strain hardening in the determination of cross-section resistances. Improved design rules (Zhao et al. 2015b, c, 2016b) have been proposed through extension of the deformation-based continuous strength method (CSM) (Ashraf et al. 2008; Gardner 2008b; Gardner et al. 2011; Afshan and Gardner 2013a; Liew and Gardner 2015; Buchanan et al. 2015) to the case of combined loading, which was shown to lead to enhanced strength predictions by allowing a rational exploitation of strain hardening. At the member level, a series of beam-column tests has been carried out on SHS and RHS members made of austenitic (Talja and Salmi 1995; Zheng et al. 2015), duplex (Huang and Young 2013; Lui et al. 2014) and ferritic (Hyttinen 1994; Zhao et al. 2016c) stainless steels, and on austenitic stainless steel CHS structural members (Burgan et al. 2000; Zhao et al. 2016d). The obtained test results generally revealed shortcomings in existing codified beam-column interaction curves, which principally stemmed from inaccurate predictions of the column buckling and bending end points of the design curves and from inaccurate interaction factors. Revised interaction factors and design formulae for stainless steel beam-columns have been proposed by Macdonald et al. (2007), Greiner and Kettler (2008), Lopes et al. (2009), Huang and Young (2015) and Zhao et al. (2016e).

The present investigation, as part of a wider study on stainless steel beam-columns by the authors, focuses on the structural behavior of stainless steel beam-column members subjected to moment gradients. A program of experiments was firstly carried out on twenty-four beam-column specimens subjected to unequal end moments. The end moment ratios were varied to provide a wide range of moment gradients along the specimen lengths. The obtained experimental data are fully reported herein, and then employed to assess the accuracy of the existing provisions given in EN 1993-1-4 (CEN 2006), SEI/ASCE-8 (ASCE 2002) and AS/NZS 4673 (AS/NZS 2001) for the design of stainless steel beam-columns subjected to moment gradients.

2. Experimental investigation

2.1 General

A test program was conducted to study the member buckling behavior of ferritic stainless steel tubular beam-columns under unequal end moments. Two cross-sections made of grade AISI 410 (EN 1.4003) stainless steel were utilized in the experiments – SHS 60×60×3 and RHS 100×40×2. Overall, the experimental program comprised a series of material tensile coupon tests to determine the material stress–strain responses of the specimens, geometric imperfection measurements to obtain the initial local and global geometric imperfections, and twenty-four beam-column tests to investigate the member buckling behavior of beam-columns subjected to unequal end moments. For each type of test, the employed experimental setup and procedures, and the test observations, including the key test results, load–deformation histories and failure modes are fully reported in the following sections.

2.2 Material testing

Prior to structural testing, a series of tensile coupon tests was conducted in order to determine the material stress–strain responses of different parts of the test specimens. For each cross-section, three coupons were tested, with two extracted from the flat portions of the specimen and one taken from the corner regions. Fig. 1 shows the locations of the coupons in the cross-section. The dimensions of the tensile coupons conformed to the requirements of the Australian Standard AS 1391 (AS 2007) and the American Standard ASTM E8M (ASTM E8M 1997). The flat coupons were 12.5 mm wide with a 50 mm gauge length while the corner coupons were 4 mm in width with a gauge length of 25 mm. The tensile coupon tests were conducted using an MTS 250 kN testing machine under displacement control at the rate of 0.05 mm/min and 0.2 mm/min up to and beyond 0.2% proof stress, respectively. The test setup consisted of an extensometer mounted onto the specimens through three-point contact knife edges and two strain gauges affixed to the mid-length of the coupons. The strain gauge readings were initially employed to determine the Young's modulus of the material and then used to calibrate the strain measurements from the extensometer. The measured tensile stress–strain curves are shown in Figs. 2 and 3 for the flat and corner coupons, respectively, while the key obtained results are reported in Tables 1 and 2. The presented material parameters include the Young's modulus E, the 0.2% proof stress $\sigma_{0.2}$, the 1.0% proof stress $\sigma_{1.0}$, the ultimate tensile strength σ_u, the strain at the ultimate tensile stress ε_u, the plastic strain at fracture ε_f measured over the standard gauge length, and the strain hardening exponents n, $n'_{0.2,1.0}$ and $n'_{0.2,u}$ used in the compound Ramberg–Osgood (R–O) material model (Ramberg and Osgood 1943; Hill 1944; Mirambell and Real 2000; Rasmussen 2003; Gardner and Ashraf 2006), as shown in Eqs (1)–(3), where $\varepsilon_{t,0.2}$ is the total strain at the 0.2% proof stress, $\varepsilon_{t,1.0}$ is the total strain at the 1.0% proof stress and $E_{0.2}$ is the tangent modulus at the 0.2% proof stress point ($\varepsilon_{t,0.2}$, $\sigma_{0.2}$). Note that Eq. (1) is the basic Ramberg–Osgood expression (Ramberg and Osgood 1943; Hill 1944), adopted up to the 0.2% proof stress, while Eq. (2) (Mirambell and Real 2000; Rasmussen 2003) and Eq. (3) (Gardner and Ashraf 2006) are the proposed second Ramberg–Osgood expressions, used beyond the 0.2% proof stress.

$$\varepsilon = \frac{\sigma}{E} + 0.002\left(\frac{\sigma}{\sigma_{0.2}}\right)^{n} \qquad \text{for } \sigma \le \sigma_{0.2} \qquad (1)$$

$$\varepsilon = \frac{\sigma - \sigma_{0.2}}{E_{0.2}} + \left(\varepsilon_u - \varepsilon_{t,0.2} - \frac{\sigma_u - \sigma_{0.2}}{E_{0.2}}\right)\left(\frac{\sigma - \sigma_{0.2}}{\sigma_u - \sigma_{0.2}}\right)^{n'_{0.2,u}} + \varepsilon_{t,0.2} \qquad \text{for } \sigma_{0.2} < \sigma \le \sigma_u \qquad (2)$$

$$\varepsilon = \frac{\sigma - \sigma_{0.2}}{E_{0.2}} + \left(\varepsilon_{t,1.0} - \varepsilon_{t,0.2} - \frac{\sigma_{1.0} - \sigma_{0.2}}{E_{0.2}}\right)\left(\frac{\sigma - \sigma_{0.2}}{\sigma_{1.0} - \sigma_{0.2}}\right)^{n'_{0.2,1.0}} + \varepsilon_{t,0.2} \qquad \text{for } \sigma_{0.2} < \sigma \le \sigma_u \qquad (3)$$

2.3 Initial geometric imperfection measurements

Initial geometric imperfections are introduced into thin-walled members primarily during the fabrication process and can significantly influence their structural performance under loading. Measurements of the initial geometric imperfections in the test specimens were therefore performed. The test setup and procedures for initial local imperfection measurements were similar to those employed by Schafer and Peköz (1998), in which, the specimen lying on the base of a milling machine, was passed under a linear variable displacement transducer (LVDT) with an accuracy of 0.001 mm, affixed to the machine head. The local imperfection measurements were not conducted specifically for each test specimen but were carried out over a representative 500 mm length of each studied cross-section size, which was away from the specimen ends to avoid measurements being overly influenced by cutting operations and end flaring due to the release of residual stresses. More detailed analyses of imperfections in stainless steel members have been carried out by Cruise and Gardner (2006). The maximum imperfection amplitude for each face was defined as the maximum deviation from a linear regression line fitted to the data set, while the maximum local imperfection amplitude of the specimen ω_0 was taken as the largest value of the measured maximum deviations from all the four faces, which was 0.024 mm and 0.033 mm for the SHS 60×60×3 and RHS 100×40×2 specimens, respectively. Figs. 4 and 5 show the measured local geometric imperfection distributions for the four faces of the two tested cross-sections. Measurements of the initial global geometric imperfection ω_g of each specimen in the direction of buckling were conducted using a theodolite and based on the readings taken at the mid-height and near the two ends of the member.

2.4 Beam-column tests

In total, twenty-four beam-columns subjected to unequal end moments were tested to investigate the buckling behavior of stainless steel beam-column structural members under axial compression and linearly varying first order bending moment (i.e., a linear moment gradient). In the experimental program, two nominal member lengths were employed for each cross-section size, with specimen lengths of 500 mm and 1250 mm for the RHS 100×40×2 members, and 600 mm and 1200 mm for the SHS 60×60×3 members. For each of the four studied member lengths, six beam-column tests, with varying end moment ratios, were carried out, leading to a total of 24 member tests. Note that, for the RHS 100×40×2 specimens, bending was induced about the minor axis. The definition of the end moment ratio ψ follows the convention in the European code EN 1993-1-1 (CEN 2005) and Nethercot and Gardner (2005), in which ψ is equal to the ratio of the smaller end moment to the larger end moment, and is taken as positive if the end moments lead to single curvature bending along the member length, but is negative if the end moments cause double curvature bending, e.g., ψ=1 represents equal but opposite end moments, which results in uniform first order bending moment and single curvature along the member length, while ψ=-1 corresponds to equal end moments, which leads to an antisymmetric triangular bending moment distribution and reverse curvature, as illustrated in Fig. 6. Note that the American specification SEI/ASCE-8

(ASCE 2002) and Australian/New Zealand standard AS/NZS 4673 (AS/NZS 2001) use an opposite sign convention with positive values of ψ for double curvature bending and negative values of ψ for single curvature bending. The following designation system was adopted for the test specimens: the designation begins with the nominal cross-section size, followed by the buckling axis (MI = minor) and nominal member length (in mm), e.g., RHS 100×40×2-MI-500. The specimens were also assigned an ID code, comprising a number and a letter (e.g., 1A): the number identifies the test series, with '1' for RHS 100×40×2-MI-500, '2' for RHS 100×40×2-MI-1250, '3' for SHS 60×60×3-600 and '4' for SHS 60×60×3-1200, and the letters from A to F indicate the varying end moment ratios employed in each test series. Measurements of the geometric dimensions and initial local imperfection amplitudes of the specimens were conducted before 25.4 mm thick end plates were welded to the member ends. The initial global geometric imperfections were, however, measured after welding in order to incorporate the effect of welding on the straightness of the specimens. All the obtained geometric parameters and initial imperfection amplitudes are reported in Table 3, where L is the member length, B is the outer cross-section width, H is the outer cross-section depth, t is the material thickness, r_i is the internal corner radius, A is the cross-section area, A_{eff} is the effective cross-section area, calculated based on the effective width method in EN 1993-1-4 (CEN 2006), and ω_0 and ω_g are the measured maximum local and global geometric imperfection amplitudes, respectively.

The beam-column tests were conducted using an AVERY 1000 kN hydraulic testing machine with pin-ended bearings at both ends, at a constant speed of 0.2 mm/min. Figs. 7(a) and 7(b) show a photograph and a schematic diagram of the beam-column experimental setup, respectively. Each pin-ended bearing consisted of a 'wedge plate' containing a knife-edge wedge, and a 'pit plate' with a V-shaped groove, as shown in Figs. 7(a) and 7(b). The specimens were firstly bolted through their end plates to the top and bottom wedge plates, which had slotted holes to allow adjustment of the relative position between the centerlines of the specimen and the knife-edges to achieve the required (nominal) loading eccentricities of e_n and ψe_n at the bottom and top ends of the members, respectively. Note that the vertical distance from the specimen end to the knife-edge was equal to 87.4 mm, and thus the member effective length L_e is calculated as the sum of the specimen length L and an additional length of 2×87.4 mm (i.e., L_e=L+87.4×2). The specimens, together with the bolted wedge plates, were then placed in the testing machine between the pit plates. The top pit plate with slotted holes was connected to the top rigid platen of the test machine through high strength bolts, and was adjusted such that the distance between the centerlines of the top and bottom pit plates was equal to e_n-ψe_n. The bottom pit plate was seated on a special bearing, which was initially free to rotate in any direction, and then restrained against twisting and rotation by tightening the vertical and horizontal bolts under a small alignment load of 2 kN. This procedure eliminates any possible gap between the knife-edges and V-grooved pit plates. An anchor device, as shown in Figs. 7(a) and 7(b), was then employed to brace the special bearing to sustain the horizontal reaction force induced by the unequal end moments through tightening the eight bolts at each side of the special bearing.

Two pairs of LVDTs positioned at both ends of the specimens were employed to determine the respective top and bottom end rotations. Two additional LVDTs were placed at the mid- and quarter-height of the specimens in order to measure the corresponding lateral deflections. Strain gauges were affixed to the extreme fibers of the cross-sections at mid- and quarter-height to capture the longitudinal strains on the maximum compressive fiber and the maximum tensile (or the minimum compressive, in some cases) fiber at these locations. The two sets of strain gauge readings were utilized to derive the actual initial loading eccentricities e_0 and ψe_0 at the bottom and top ends of the members, respectively. The calculation procedures to determine e_0 and ψe_0 are as follows. Firstly, the initial global geometric imperfection pattern is assumed to be sinusoidal with a maximum value of ω_g at mid-height, as defined by Eq. (4). The global imperfection amplitude at the quarter-height of the specimens $\omega_{L/4}$ is thus equal to $\omega_g \sin\left[\pi\left(L_e/2-L/4\right)/L_e\right]$, where L is the specimen length and L_e is the effective member length.

$$\omega(x)=\omega_g \sin\left(\frac{\pi x}{L_e}\right) \tag{4}$$

During testing, the induced horizontal reaction force F at each end of the member can be calculated from Eq. (5).

$$F=\frac{Ne_0-Ne_0\psi}{L_e} \tag{5}$$

The resultant bending moments at the quarter-height $M_{L/4}$ and mid-height $M_{L/2}$ of the specimens, resulting from the horizontal reaction force and eccentric axial force, are determined from Eq. (6) and Eq. (7), where $\kappa_{L/4}$ and $\kappa_{L/2}$ are the curvatures at the quarter- and mid-height of the specimens, respectively, $\delta_{L/4}$ and $\delta_{L/2}$ are the corresponding lateral deflection measurements from the LVDTs, and $\omega_{L/4}=\omega_g \sin\left[\pi\left(L_e/2-L/4\right)/L_e\right]$ and $\omega_{L/2}=\omega_g$ are the initial global imperfection amplitudes at each location.

$$M_{L/4}=EI\kappa_{L/4}=N\left(\omega_{L/4}+e_0+\delta_{L/4}\right)-\frac{\left(Ne_0-Ne_0\psi\right)}{L_e}\left(\frac{L_e}{2}-\frac{L}{4}\right) \tag{6}$$

$$M_{L/2}=EI\kappa_{L/2}=N\left(\omega_{L/2}+e_0+\delta_{L/2}\right)-\frac{\left(Ne_0-Ne_0\psi\right)}{L_e}\left(\frac{L_e}{2}\right) \tag{7}$$

As indicated by the authors in previous research on beam-columns (Huang and Young 2013; Zhao et al. 2016c, d), the measured longitudinal strains at the quarter- and mid-height of the specimens are made up of two components: (i) strains due to the applied compressive load $\varepsilon_c = \left(\varepsilon_{max} + \varepsilon_{min}\right)/2$, and (ii) strains due to the corresponding bending moment $\varepsilon_b = \left(\varepsilon_{max} - \varepsilon_{min}\right)/2$, where ε_{max} and ε_{min} are the strain gauge values of the maximum compressive fiber and the maximum tensile (or the minimum compressive, in some cases) fiber, respectively. Thus, the curvatures at the quarter- and mid-height of the specimens $\kappa_{L/4}$ and $\kappa_{L/2}$ are equal to $\varepsilon_{b,L/4}/(0.5H)$ and $\varepsilon_{b,L/2}/(0.5H)$, respectively, where $\varepsilon_{b,L/4}$ and $\varepsilon_{b,L/2}$ are the strains due to the bending moments at the quarter-height and mid-height of the specimens.

The initial loading eccentricity at the bottom end of the member e_0 and the end moment ratio ψ can then be calculated by solving Eq. (6) and Eq. (7) simultaneously, as given by Eq. (8) and Eq. (9).

$$e_0 = 2L_e/L\left(EI\kappa_{L/4}/N - \omega_{L/4} - \delta_{L/4}\right) - \left(2L_e/L - 1\right)\left(EI\kappa_{L/2}/N - \omega_{L/2} - \delta_{L/2}\right) \tag{8}$$

$$\psi = \frac{\left(2L_e/L + 1\right)\left(EI\kappa_{L/2}/N - \omega_{L/2} - \delta_{L/2}\right) - 2L_e/L\left(EI\kappa_{L/4}/N - \omega_{L/4} - \delta_{L/4}\right)}{2L_e/L\left(EI\kappa_{L/4}/N - \omega_{L/4} - \delta_{L/4}\right) - \left(2L_e/L - 1\right)\left(EI\kappa_{L/2}/N - \omega_{L/2} - \delta_{L/2}\right)?} \tag{9}$$

Note that the initial loading eccentricity and end moment ratio for each of the test specimens were determined as the average calculated values during the early stages of loading (the authors suggest using no more than 15% of the ultimate load), where the structural behavior was very close to linear and elastic.

The key experimental results obtained for each test series are reported in Table 4, where L_e is the effective member length, $\bar{\lambda}=\sqrt{A_{eff}\sigma_{0.2}/N_{cr}}$ is the non-dimensional column slenderness, where N_{cr} is the Euler buckling load about the considered axis of buckling, e_0 is the initial calculated loading eccentricity at the bottom end of the member determined according to Eq. (8), ψ is the end moment ratio, determined according to Eq. (9), N_u is the ultimate test load, $M_{u,b}= N_u e_0$ and $M_{u,t}= N_u e_0 \psi$ are the ultimate test bottom and top end moments, respectively, $\phi_{u,b}$ and $\phi_{u,t}$ are the corresponding bottom and top end rotations at the ultimate load, and $\delta_{u,L/2}$ and $\delta_{u,L/4}$ are the mid- and quarter-height lateral deflections at the ultimate load, respectively. For each test series, the full experimental load–lateral deflection curves at the mid-height and quarter-height of the specimens are shown in Figs. 8–11. In terms of failure modes, the more compact SHS 60×60×3 specimens generally exhibited global buckling, while the more slender RHS 100×40×2 specimens showed an interaction of global and local buckling. For each test series, the critical cross-section could be seen to migrate from the member ends to the mid-height of the specimens, as the end moment ratio varied from -1 (antisymmetric triangular first order bending moment distribution) to 1 (uniform first order bending moment distribution), as shown in the typical failure modes presented in Figs. 12 and 13.

3. Discussion and assessment of current design methods

3.1 General

In this section, the established codified design provisions for stainless steel beam-column structural members subjected to moment gradient, set out in the European code EN 1993-1-4 (CEN 2006), American specification SEI/ASCE-8 (ASCE 2002) and Australian/New Zealand standard AS/NZS 4673 (AS/NZS 2001), are introduced and discussed. The accuracy of each codified approach is then assessed through comparisons of the test beam-column strengths with the predicted strengths. The comparisons are presented in terms of the failure load ratio, $N_u/N_{u,pred}$ (Zhao et al. 2015c, 2016b, c, d), of which the definition is illustrated in Fig. 14, where N_u is the test axial load, while $N_{u,pred}$ is the predicted axial load corresponding to the intersection of the line between the origin and the test point with the design interaction curve, assuming proportional loading. Table 5 reports the ratios of test to predicted failure loads for each design method; ratios greater than unity indicate that the test data points lie on the safe side of the design interaction curve. Note that all calculations have been made based on the measured material and geometric properties of the test specimens and with partial factors set equal to unity.

3.2 European code EN 1993-1-4 (EC3)

The European code EN 1993-1-4 (CEN 2006) for stainless steel structures employs the same design formula for beam-columns subjected to both equal and unequal end moments, without taking into account the beneficial effect of the moment gradient on the global stability of beam-columns; this rather conservative approach is partly due to the lack of experimental data at the time of the development of the European code for structural stainless steel. The design formula for stainless steel tubular section beam-columns under equal and unequal end moment is given by Eq. (10), where N_{Ed} is the design axial load, $M_{Ed}= N_{Ed}e_0$ is the design bending moment about the considered axis of buckling, defined as the maximum first order bending moment induced by the applied unequal end moments, $N_{b,Rd}$ is the codified column buckling strength, determined according to Clause 5.4.2 of EN 1993-1-4 for uniform members in compression, e_N is the shift in the neutral axis when slender cross-sections are subjected to uniform compression, which is equal to zero for doubly symmetric SHS and

RHS, W_{pl} is the plastic section modulus about the axis of buckling, β_W is a factor that is equal to unity for Class 1 or 2 sections, the ratio of elastic to plastic moduli for Class 3 sections and the ratio of effective to plastic moduli for Class 4 cross-sections, and k is the buckling interaction factor, as defined by Eq. (11).

$$\frac{N_{Ed}}{N_{b,Rd}} + k\left(\frac{M_{Ed} + N_{Ed}e_N}{\beta_W W_{pl}\sigma_{0.2}}\right) \leq 1 \tag{10}$$

$$1.2 \leq k = 1 + 2\left(\bar{\lambda} - 0.5\right)\frac{N_{Ed}}{N_{b,Rd}} \leq 1.2 + 2\frac{N_{Ed}}{N_{b,Rd}} \tag{11}$$

The accuracy of the EN 1993-1-4 design rules for ferritic stainless steel beam-columns subjected to unequal end moments is evaluated by comparing the experimental results with the predicted strengths. The comparisons, as reported in Table 5, show that the mean ratio of test to EC3 predicted strengths $N_u/N_{u,EC3}$ is equal to 1.48 with a coefficient of variation (COV) equal to 0.18, revealing a high degree of conservatism and scatter in the strength predictions. It may also be observed from each test series that the conservatism increases as the end moment ratio varies from 1 (i.e., uniform first order moment distribution) to -1 (i.e., antisymmetric triangular first order moment distribution), which generally highlights the weakness of treating beam-columns subjected to both equal and unequal end moments in the same manner; this can also be seen in Fig. 15, where the ratio of test to EC3 capacities is plotted against the end moment ratio ψ for each test series.

The introduction of equivalent moment factors into the Eurocode stainless steel beam-column design formula was thus investigated. Two equivalent moment factors, as used for carbon steel beam-columns in EN 1993-1-1 (CEN 2005), were assessed. The first one, given by Eq. (12), is known as the equivalent uniform moment factor $C_{m,u}$ (Austin 1961; Lindner 2003; Greiner and Lindner 2006; Boissonnade et al. 2006), which was derived based on a constant reference moment, while the second one, shown in Eq. (13), is called the equivalent sinusoidal moment factor $C_{m,s}$ (Boissonnade et al. 2002, 2004, 2006), developed on the basis of a sinusoidal reference moment. Similarly to the interaction factor k, which depends on the non-dimensional slenderness $\bar{\lambda}$ and the applied axial load level $n=N_{Ed}/N_{b,Rd}$, the equivalent moment factor, accounting for the influence of non-uniform bending moments along the member length, is also dependent on the level of coexistent axial load and is therefore a function of $\bar{\lambda}$ and n, as well as the end moment ratio ψ. However, the effect of $\bar{\lambda}$ and n is generally neglected in the determination of equivalent uniform moment factors $C_{m,u}$, as shown in Eq. (12), though it was considered in the development of the equivalent sinusoidal moment factor $C_{m,s}$ (Eq. (13)), which may lead to more accurate equivalence. Note that a lower bound limit of 0.4 is employed for the equivalent uniform moment factor $C_{m,u}$ in Eq. (12), in order to prevent underestimations of the equivalent bending moment and thus over-predictions of the beam-column strengths. Comparisons between the equivalent uniform and sinusoidal moment factors determined respectively from Eq. (12) and Eq. (13) are shown in Fig. 16, where both factors are plotted against the ratio of N_{Ed}/N_{cr} for varying end moment ratios ψ.

$$C_{m,u} = 0.6 + 0.4\psi \geq 0.4 \tag{12}$$

$$C_{m,s} = 0.79 + 0.21\psi + 0.36(\psi - 0.33)\frac{N_{Ed}}{N_{cr}} \tag{13}$$

Use of both equivalent moment factors in Eq. (10) (i.e. by multiplying the bending term in Eq. (10) by $C_{m,u}$ or $C_{m,s}$) is assessed in Table 5, where $N_u/N_{u,EC3\text{-}U}$ and $N_u/N_{u,EC3\text{-}S}$ indicate the ratios of test to predicted failure loads calculated through the use of $C_{m,u}$ and $C_{m,s}$, respectively. The results show that the mean ratio of test to predicted failure loads decreases from 1.43 to 1.18 and the COV decreases from 0.18 to 0.13 if $C_{m,u}$ was employed, while the adoption of $C_{m,s}$ results in a decrease in the mean ratio from 1.43 to 1.28 and a decrease of the COV from 0.18 to 0.13, both of which represent substantial improvements in the prediction of stainless steel beam-column strengths under moment gradients, though further experimental and numerical verification is required.

3.3 American Specification SEI/ASCE-8

The American specification SEI/ASCE-8 (ASCE 2002) considers the influence of moment gradient in the design of beam-columns subjected to unequal end moments, through use of an equivalent uniform moment factor. The design formula, derived on the basis of second-order elastic theory, is given by Eq. (14), where N_n is the column buckling strength, calculated in accordance with Clause 3.4 of SEI/ASCE-8 (ASCE 2002), which employs the tangent modulus approach to account for the nonlinear material response and gradual yielding of stainless steel in the design of column members, and M_n is the codified bending resistance calculated according to Clause 3.3.1.1, in which Procedure II, utilizing the inelastic reserve capacity, is employed for the determination of the cross-section bending moment resistance of the non-slender cross-sections. Note that the inelastic reserve capacity provisions only account for partial plasticity, and the calculated bending resistances are therefore always less than the plastic moment capacity M_{pl}. The other terms in Eq. (14) are C_m and α_n. C_m=0.6+0.4ψ is the classic equivalent uniform moment factor, which is equal to unity for a beam-column subjected to equal end moments (i.e., ψ=1), leading to uniform first order bending moment along the member length, and is less than unity for unequal end moments (i.e., $-1 \leq \psi < 1$), resulting in linearly varying bending moment along the length of the beam-column, and α_n is the magnification factor equal to $(1\text{-}N_{Ed}/N_{cr})$ to approximate the second order bending moment.

$$\frac{N_{Ed}}{N_n}+\frac{C_m M_{Ed}}{M_n \alpha_n}\leq 1 \tag{14}$$

The test strengths of the beam-columns under moment gradient are compared against the capacity predictions of SEI/ASCE-8 (ASCE 2002) in Table 5. The comparisons show that the American specification leads to a high level of accuracy and consistency in the strength predictions on average, with the mean $N_u/N_{u,ASCE}$ ratio equal to 1.07 and a COV of 0.06. However, SEI/ASCE-8 also results in unsafe predictions for beam-columns subjected to high moment gradients, e.g., specimen RHS 100×40×2-MI-500-1A with ψ=-0.59 and specimen SHS 60×60×3-600-1A with ψ=-0.66, which may be due to an overestimation of the beneficial effect of the non-uniform bending moment distribution on the beam-column stability. The European code for carbon steel EN 1993-1-1 (CEN 2005) employs the same expression for the equivalent uniform moment factor but assumes no further benefits are obtained for ψ values smaller than -0.5. This is achieved by placing a lower limit of 0.4 on the C_m factor. Comparisons between the equivalent uniform moment factors from the European code and American specification are presented in Fig. 17. Use of 0.4 as the lower limit value of the C_m factor in SEI/ASCE-8 (ASCE 2002) was also evaluated. The results showed that the $N_u/N_{u,ASCE}$ ratios increased from 0.96 to 0.98, and 0.97 to 0.99 for specimens RHS 100×40×2-MI-500-1A and SHS 60×60×3-600-1A, respectively, indicating reduced unconservatism in the predictions. The remaining unconservatism may result from over-prediction of the column buckling end point of the design beam-column interaction curve (Zhao et al. 2016c).

3.4 Australian/New Zealand standard AS/NZS 4673

The Australian/New Zealand standard AS/NZS 4673 (AS/NZS 2001) employs the same beam-column design formula as the American specification SEI/ASCE-8 (ASCE 2002), but adopts different provisions for the determination of bending moment capacities and column buckling strengths. With regards to bending moment capacities, both codes employ the inelastic reserve capacity approach, but the Australian/New Zealand standard allows use of the full plastic moment capacity below a specified slenderness limit. For the calculation of column buckling strengths, an explicit method (Rasmussen and Rondal 1997), developed based on the Perry-Robertson buckling formulation with a series of imperfection parameters for different stainless steel grades to account for the differing levels of nonlinearity, is provided in AS/NZS 4673 (AS/NZS 2001) as an alternative to the tangent modulus method. As highlighted by Afshan and Gardner (2013b) and Zhao et al. (2016c), the tangent modulus method often results in unsafe column buckling strength predictions, while the use of the explicit method leads to more conservative but safe strength predictions. Thus, the AS/NZS 4673 beam-column design formula (AS/NZS 2001) maintains the general format of Eq. (14) but with the more conservative column buckling strength predictions N_a and more accurate bending moment capacity predictions M_a, replacing those from the American specification.

A numerical evaluation of the Australian/New Zealand standard AS/NZS 4673 (AS/NZS 2001) is reported in Table 5, showing that, overall, AS/NZS 4673 yields slightly less accurate capacity predictions than SEI/ASCE-8, with the mean ratio of test to predicted strengths equal to 1.16, and similar scatter, with the COV equal to 0.06, but all the predictions now lie on the safe side. This can also be seen in Fig. 18, where the ratios of test beam-column strengths to predicted strengths from the American specification and Australian/New Zealand standard are plotted against the end moment ratio ψ.

3.5 Summary

Overall, the European code EN 1993-1-4 (CEN 2006) leads to the most conservative and scattered strength predictions among the considered codified methods; this is mainly due to the lack of consideration of the moment gradient in the design of stainless steel beam-columns subjected to unequal end moments. Use of two equivalent moment factors in the Eurocode stainless steel beam-column formula was also assessed, and shown to result in more accurate and consistent capacity predictions. The American specification SEI/ASCE-8 (ASCE 2002) and Australian/New Zealand standard AS/NZS 4673 (AS/NZS 2001) employ an equivalent uniform moment factor to account for the moment gradient in the design of beam-columns. The SEI/ASCE-8 yielded a high level of accuracy and consistency in the prediction of beam-column strengths under unequal end moments, on average, but with some unsafe predictions for beam-columns subjected to high moment gradients. The Australian/New Zealand standard was found to offer the most suitable design provisions, leading to safe but slightly conservative predictions. Comparisons between the three codified methods are shown in Fig. 19, where the test beam-column strengths are plotted against the predicted strengths. Overall, all the current existing design provisions for stainless steel beam-columns subjected to unequal end moments exhibit some shortcomings, and a comprehensive numerical study for the development of improved provisions is therefore underway as part of a wider study.

4. Conclusions

A comprehensive experimental study of ferritic stainless steel tubular section beam-columns subjected to moment gradients has been conducted. The test program included material tensile coupon tests, initial local and global imperfection measurements and twenty-four beam-columns tests under unequal end moments. The end moment ratios were varied to enable a wide range of moment gradients to be examined. The test setup and experimental procedures for each type of test have been fully described. Key test results, including the ultimate loads and the corresponding deformation parameters at the ultimate loads have been tabulated, while the full load–deformation histories and typical buckling modes of the test specimens have also been presented. The experimental results were carefully analyzed and then used to evaluate the accuracy of the current established design methods for beam-columns subjected to unequal end moments, given in the European code EN 1993-1-4 (CEN 2006), American specification SEI/ASCE-8 (ASCE 2002), and Australia and New Zealand standard AS/NZS 4673 (AS/NZS 2001). Generally, the European code, which neglects the effect of moment gradient in the design of beam-columns under unequal end moments, was found to give the most conservative and scattered strength predictions among the three methods. The American specification and Australian/New Zealand standard employ an equivalent uniform moment factor in the determination of beam-column strengths under non-uniformly distributed bending moment, which leads to an increased level of accuracy on average, but with some unsafe predictions from SEI/ASCE-8 (ASCE 2002) and some unduly conservative predictions from AS/NZS 4673 (AS/NZS 2001). Therefore, it is concluded that improvements in the design of stainless steel beam-columns subjected to moment gradients are required, and further research is underway in this area.

Acknowledgements

The authors are grateful to the Joint PhD Scholarship Program from Imperial College London and the University of Hong Kong for its financial support, and would also like to thank Mr. Man Lai Wong from the University of Hong Kong for his contribution to the experimental investigations.

References

Afshan, S., and Gardner, L. (2013a). "The continuous strength method for structural stainless steel design." *Thin-Walled Struct*., 68(4), 42–49.

Afshan, S., and Gardner, L. (2013b). "Experimental study of cold-formed ferritic stainless steel hollow sections." *J. Struct. Eng*., 139(5), 717–728.

Arrayago, I., and Real, E. (2015). "Experimental study on ferritic stainless steel RHS and SHS cross-sectional resistance under combined loading." *Structures*, accepted.

AS. (2007). "Metallic materials – tensile testing at ambient temperature." *AS 1391-2007*, Sydney.

ASCE. (2002). "Specification for the design of cold-formed stainless steel structural members." *SEI/ASCE 8-02*, Reston, VA.

Ashraf, M., Gardner, L., and Nethercot, D. A. (2008). "Structural stainless steel design: resistance based on deformation capacity." *J. Struct. Eng*., 134(3), 402–411.

AS/NZS. (2001). “Cold-formed stainless steel structures.” *AS/NZS 4673:2001*, Sydney.

ASTM E8M. (1997). “Standard test methods for tension testing for metallic materials.” *E8M-97*, West Conshohocken, USA.

Austin, W. J. (1961). “Strength and design of metal beam-columns.” *J. Struct. Div.*, 87(4), 1–34.

Boissonnade, N., Greiner, R., Jaspart, J-P., and Lindner, J. (2006). “Rules for Member Stability in EN 1993-1-1: Background documentation and design guidelines.” *ECCS European Convention for Constructional Steelwork*.

Boissonnade, N., Jaspart, J-P., Muzeau, J-P., and Villette, M. (2002). “Improvement of the interaction formulae for beam columns in Eurocode 3.” *Comput. Struct.*, 80(27), 2375–2385.

Boissonnade, N., Jaspart, J-P., Muzeau, J-P., and Villette, M. (2004). “New Interaction formulae for beam-columns in Eurocode 3. The French–Belgian approach.” *J. Constr. Steel Res.*, 60, 421–431.

Buchanan, C., Gardner, L., and Liew, A. (2015). “The continuous strength method for the design of circular hollow sections.” *J. Constr. Steel Res.*, submitted.

Burgan, B. A., Baddoo, N. R., and Gilsenan, K. A. (2000). “Structural design of stainless steel members – comparison between Eurocode 3, Part 1.4 and test results.” *J. Constr. Steel Res.*, 54(1), 51–73.

CEN. (2005). “Design of steel structures: Part 1-1: General rules and rules for buildings.” *Eurocode 3*, *EN 1993-1-1*, Brussels, Belgium.

CEN. (2006). “Design of steel structures: Part 1-4: General rules: Supplementary rules for stainless steel.” *Eurocode 3*, *EN 1993-1-4*, Brussels, Belgium.

Cruise, R. B., and Gardner, L. (2006). “Measurement and prediction of geometric imperfections in structural stainless steel members.” *Struct. Eng. Mech.*, 24(1), 63–89.

Gardner, L. (2008a). “Aesthetics, economics and design of stainless steel structures.” *Adv. Steel Constr.*, 4(2), 113–122.

Gardner, L. (2008b). “The Continuous Strength Method.” *Proc. ICE Struct. Build.*, 161(3), 127–133.

Gardner, L., and Ashraf, M. (2006). “Structural design for non-linear metallic materials.” *Eng. Struct.*, 28(6), 926–934.

Gardner, L., Wang, F., and Liew, A. (2011). “Influence of strain hardening on the behavior and design of steel structures.” *Int. J. Struct. Stab. Dyn.*, 11(5), 855–875.

Greiner, R., and Kettler, M. (2008). “Interaction of bending and axial compression of stainless steel members.” *J. Constr. Steel Res.*, 64(11), 1217–1224.

Greiner, R., and Lindner, J. (2006). “Interaction formulae for members subjected to bending and axial compression in EUROCODE 3 – the Method 2 approach.” *J. Constr. Steel Res.*, 62(8), 757–770.

Hill, H. N. (1944). “Determination of stress–strain relations from offset yield strength values.” *Tech. Note 927*, National advisory committee for aeronautics, Washington, DC.

Huang, Y., and Young, B. (2013). “Experimental and numerical investigation of cold-formed lean duplex stainless steel flexural members.” *Thin-Walled Struct.*, 73(19), 216–228.

Huang, Y., and Young, B. (2015). “Design of cold-formed lean duplex stainless steel members in compression and bending.” *J. Struct. Eng.*, 10.1061/(ASCE)ST.1943–541X.0001091, 04014138.

Hyttinen, V. (1994). “Design of cold-formed stainless steel SHS beam-columns.” *Rep. 41*, Univ. of Oulu, Oulu, Finland.

Liew, A., and Gardner, L. (2015). “Ultimate capacity of structural steel cross-sections under compression, bending and combined loading.” *Structures*, 1, 2–11.

Lindner, J. (2003). “Design of beams and beam columns.” *Prog. Struct. Eng. Mat.*, 5(1), 38–47.

Lopes, N., Vila Real, P., and Simões da Silva, L. (2009). “Stainless steel beam-columns interaction curves with and without lateral torsional buckling.” *Proc. 7th EUROMECH Solid Mech. Conf.*, Lisbon, Portugal.

Lui, W. M., Ashraf, M., and Young, B. (2014). “Tests of cold-formed duplex stainless steel SHS beam-columns.” *Eng. Struct.*, 74, 111–121.

Macdonald, M., Rhodes, J., and Kotelko, M. (2007) “Stainless steel stub columns subject to combined bending and axial loading.” *Thin-Walled Struct.*, 45(10), 893–897.

Mirambell, E., and Real, E. (2000). “On the calculation of deflections in structural stainless steel beams: An experimental and numerical investigation.” *J. Constr. Steel Res.*, 54(1), 109–133.

Nethercot, D. A., and Gardner, L. (2005). “The EC3 approach to the design of columns, beams and beam-columns.” *Steel Compos. Struct.*, 5(2–3), 127–140.

Ramberg, W., and Osgood, W. R. (1943). “Description of stress–strain curves by three parameters.” *Tech. Note 902*, National advisory committee for aeronautics, Washington, DC.

Rasmussen, K. J. R., and Rondal, J. (1997). “Strength curves for metal columns.” *J. Struct. Eng.*, 123(6), 721–728.

Rasmussen, K. J. R. (2003). “Full-range stress-strain curves for stainless steel alloys.” *J. Constr. Steel Res.*, 59(1), 47–61.

Schafer, B. W., and Peköz, T. (1998). “Computational modelling of cold-formed steel: Characterizing geometric imperfections and residual stresses.” *J. Constr. Steel Res.*, 47(3), 193–210.

Talja, A., and Salmi, P. (1995). “Design of stainless steel RHS beams, columns and beam-columns.” *VTT Research Note 1619*, Technical Research Centre of Finland, Finland.

Zhao, O., Rossi, B., Gardner, L., and Young, B. (2015a). “Behaviour of structural stainless steel cross-sections under combined loading – Part I: Experimental study.” *Eng. Struct.*, 89, 236–246.

Zhao, O., Rossi, B., Gardner, L., and Young, B. (2015b). "Behaviour of structural stainless steel cross-sections under combined loading – Part II: Numerical modelling and design approach." *Eng. Struct.*, 89, 247–259.

Zhao, O., Rossi, B., Gardner, L., and Young, B. (2015c). "Experimental and numerical studies of ferritic stainless steel tubular cross-sections under combined compression and bending." *J. Struct. Eng.*, 10.1061/(ASCE)ST.1943-541X.0001366, 04015110.

Zhao, O., Gardner, L., and Young, B. (2016a). "Structural performance of stainless steel circular hollow sections under combined axial load and bending – Part 1: Experiments and numerical modelling." *Thin-Walled Struct.*, http://dx.doi.org/10.1016/j.tws.2015.12.003.

Zhao, O., Gardner, L., and Young, B. (2016b). "Structural performance of stainless steel circular hollow sections under combined axial load and bending – Part 2: Parametric studies and design." *Thin-Walled Struct.*, http://dx.doi.org/10.1016/j.tws.2015.12.005.

Zhao, O., Gardner, L., and Young, B. (2016c). "Buckling of ferritic stainless steel members under combined axial compression and bending." *J. Constr. Steel Res.*, 117, 35–48.

Zhao, O., Gardner, L., and Young, B. (2016d). "Testing and numerical modelling of austenitic stainless steel CHS beam-columns." *Eng. Struct.*, 111, 263–274.

Zhao, O., Gardner, L., and Young, B. (2016e). "Behaviour and design of stainless steel SHS and RHS beam-columns." *J. Constr. Steel Res.*, submitted.

Zheng, B., Hua, X., and Shu, G. (2015). "Tests of cold-formed and welded stainless steel beam-columns." *J. Constr. Steel Res.*, 111, 1–10.

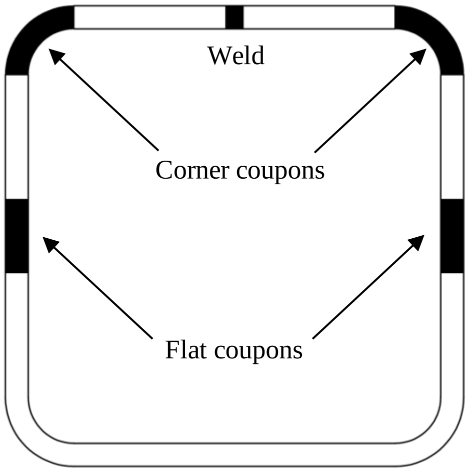

Fig. 1. Locations of coupons in the cross-section.

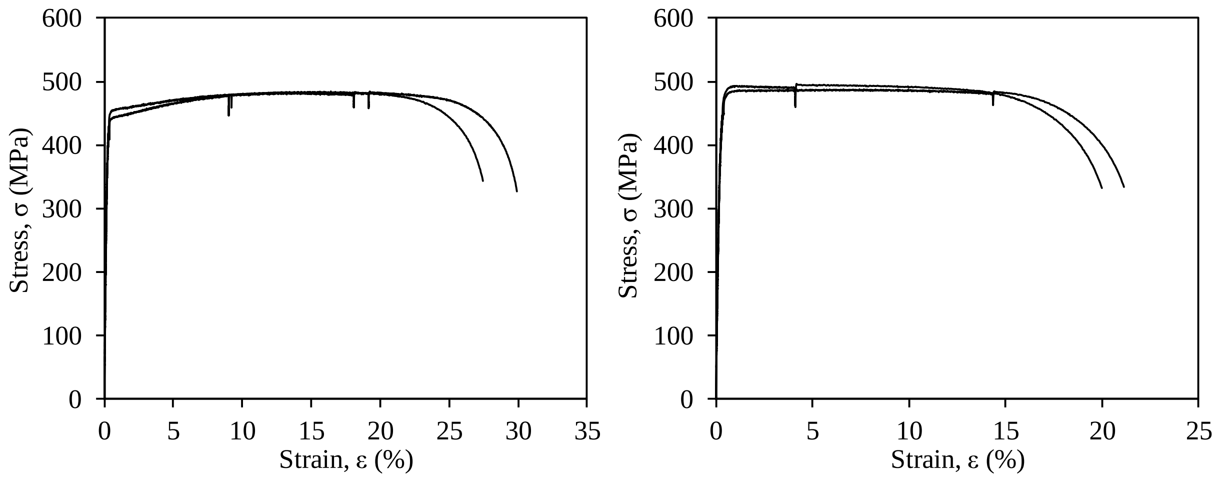

(a) RHS 100×40×2.

(b) SHS 60×60×3.

Fig. 2. Material stress–strain curves from flat coupon tests.

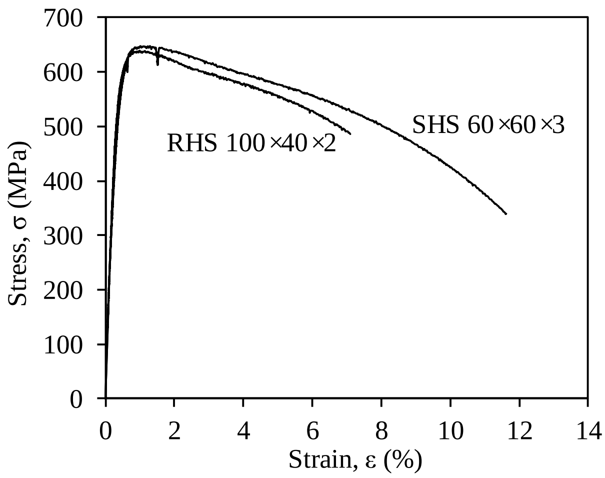

Fig. 3. Material stress–strain curves from corner coupon tests.

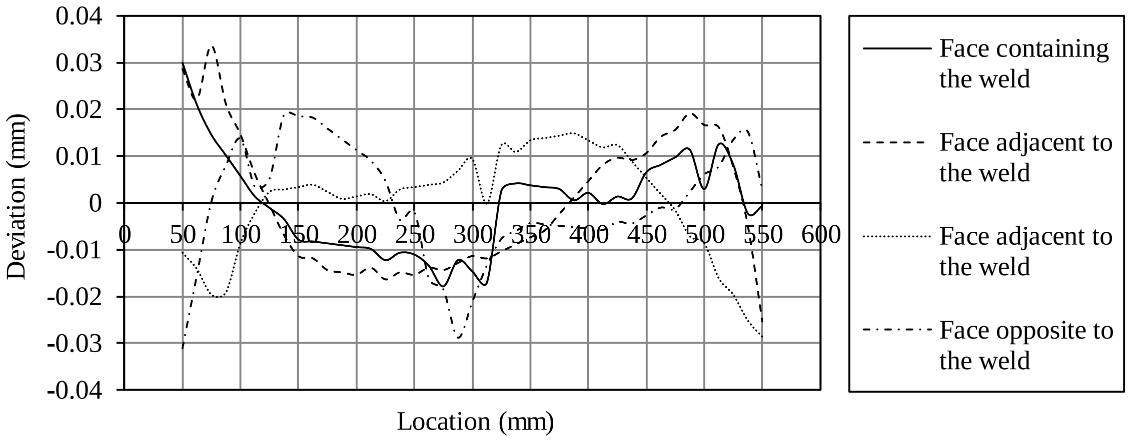

Fig. 4. Measured local geometric imperfection distributions for the RHS 100×40×2 specimen.

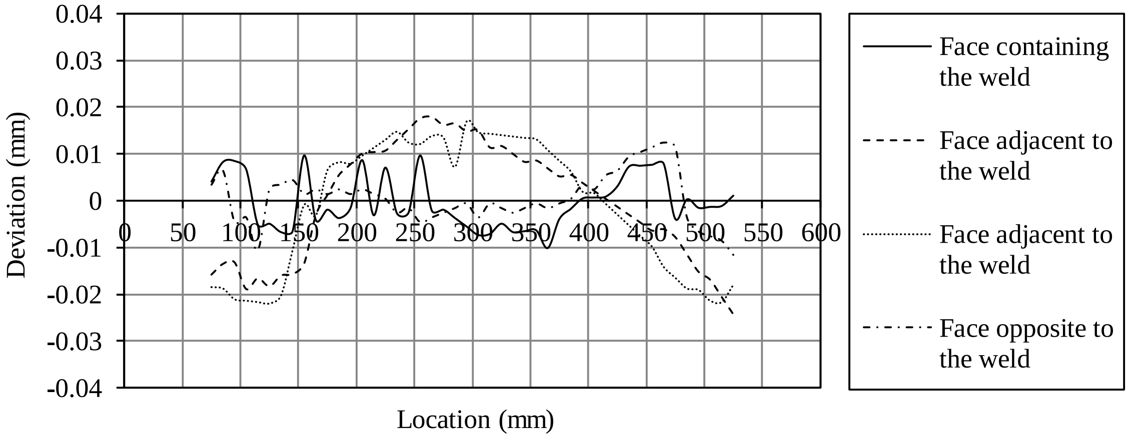

Fig. 5. Measured local geometric imperfection distributions for the SHS 60×60×3 specimen.

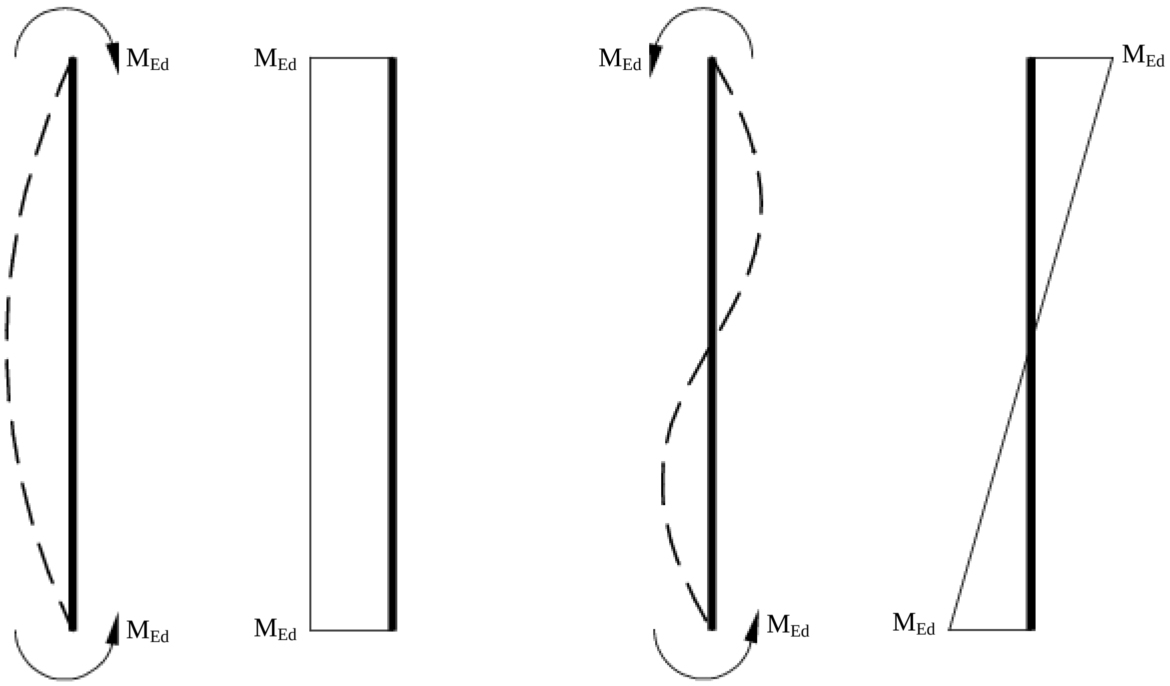

(a) ψ=1. (b) ψ=-1.

Fig. 6. Illustration of end moment ratio ψ.

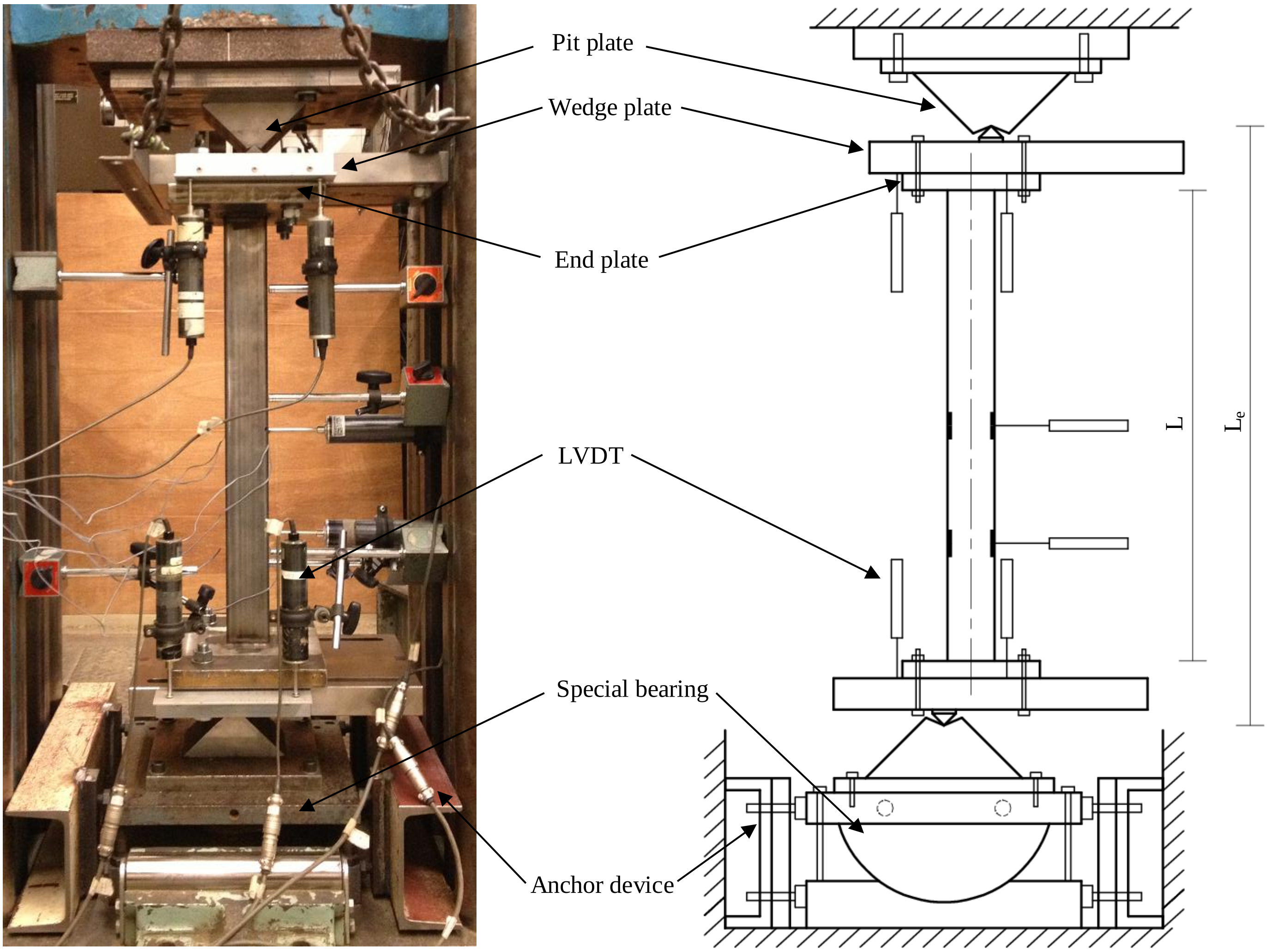

(a) Experimental setup.

(b) Schematic diagram of the test setup.

Fig. 7. Beam-column test configuration.

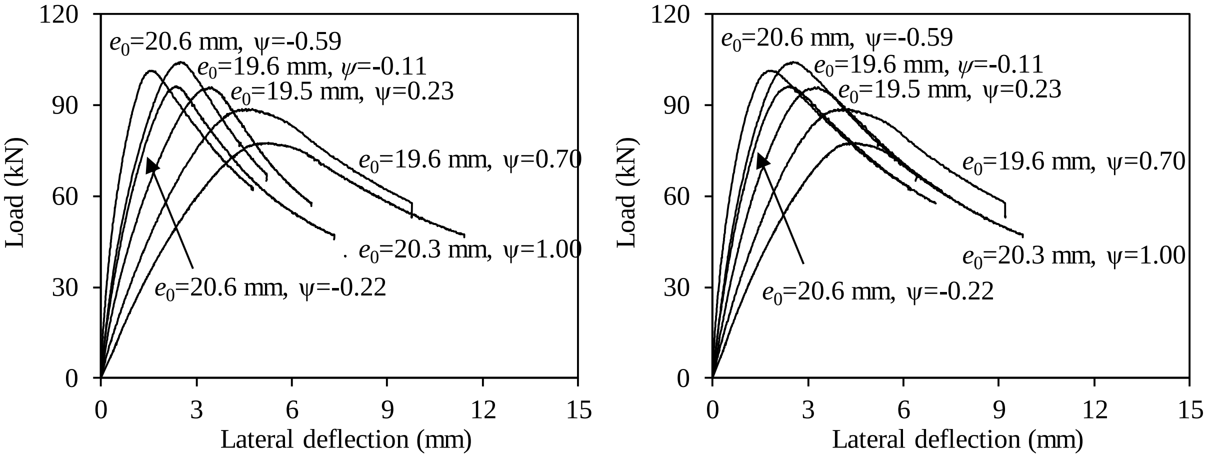

(a) At mid-height. (b) At quarter-height

Fig. 8. Load–lateral deflection curves for RHS 100×40×2-500 specimens.

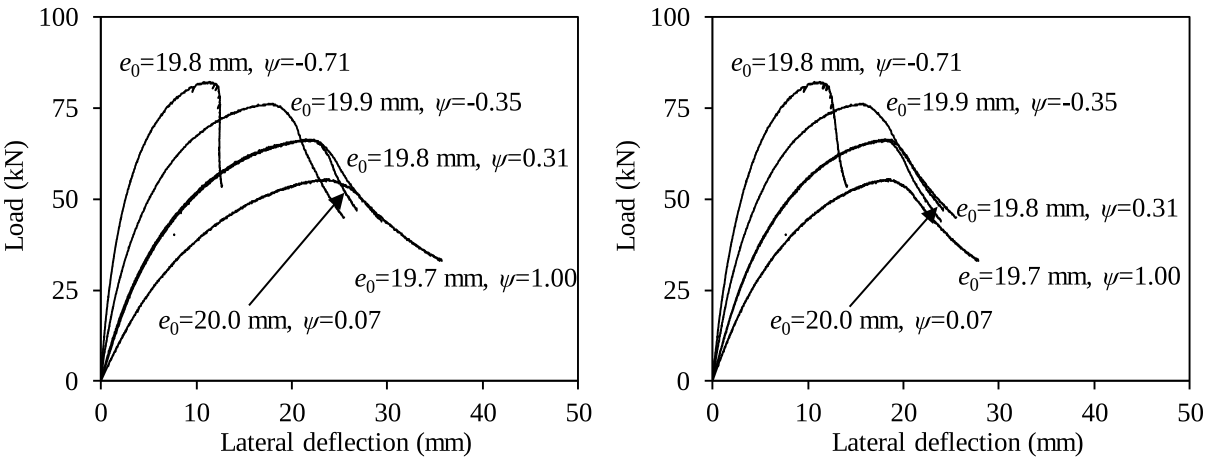

(a) At mid-height. (b) At quarter-height.

Fig. 9. Load–lateral deflection curves for RHS 100×40×2-1250 specimens.

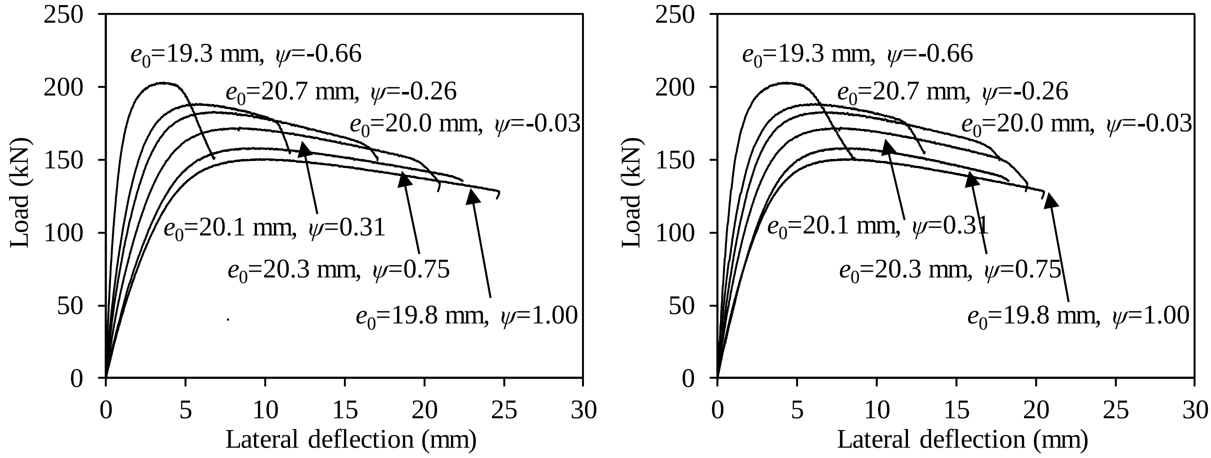

(a) At mid-height. (b) At quarter-height.

Fig. 10. Load–lateral deflection curves for SHS 60×60×3-600 specimens.

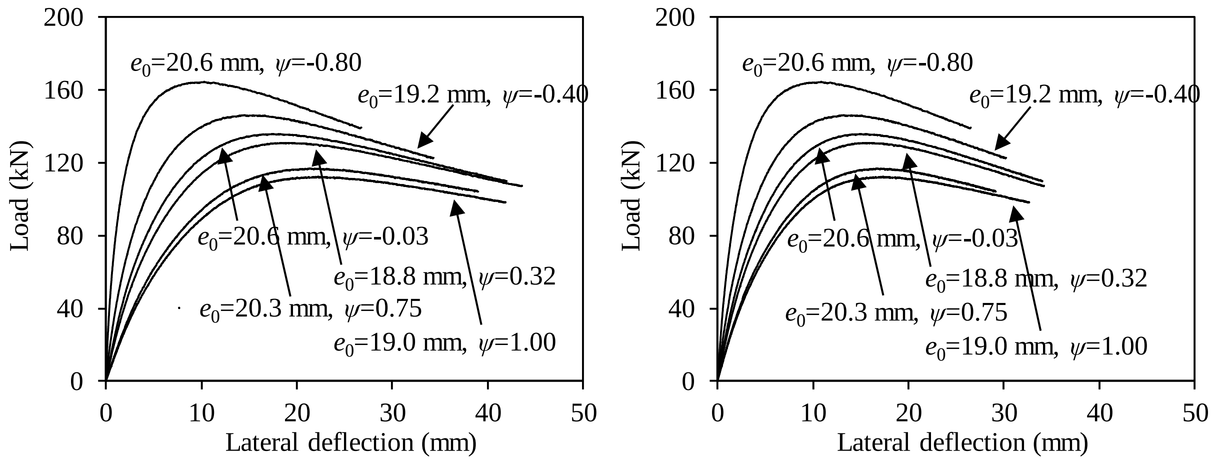

(a) At mid-height. (b) At quarter-height.

Fig. 11. Load–lateral deflection curves for SHS 60×60×3-1200 specimens.

Fig. 12. Experimental failure modes for RHS 100×40×2-MI-1250 specimens (from left to right, the end moment ratios ψ are equal to -0.71, -0.35, 0.07, 0.31, 0.75 and 1.00).

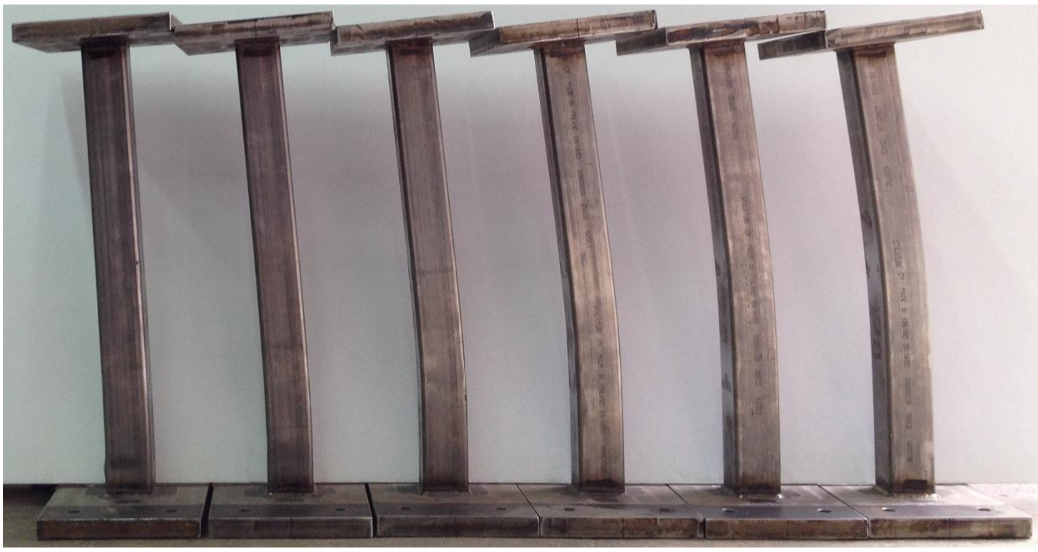

Fig. 13. Experimental failure modes for SHS 60×60×3-600 specimens (from left to right, the end moment ratios ψ are equal to -0.66, -0.26, -0.03, 0.31, 0.75 and 1.00).

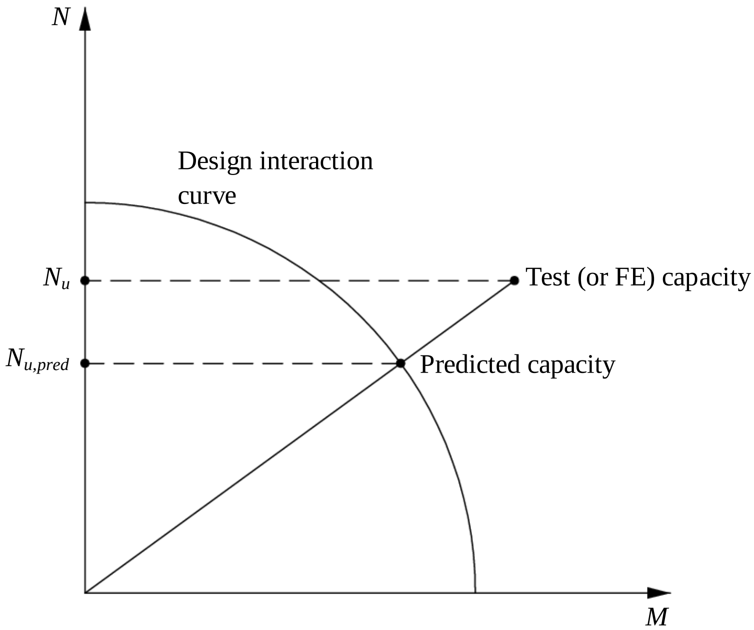

Fig. 14. Definition of N_u and $N_{u,pred}$ on axial load–moment interaction curve.

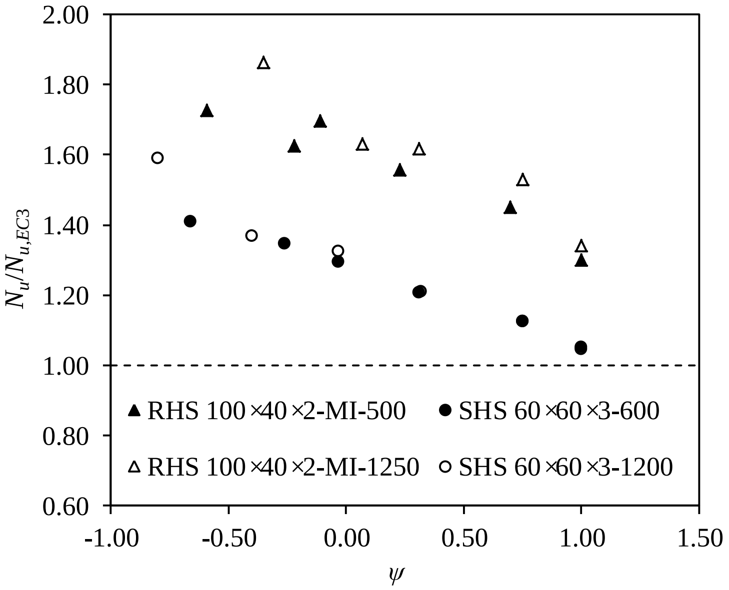

Fig. 15. Comparison of test results with EN 1993-1-4 strength predictions

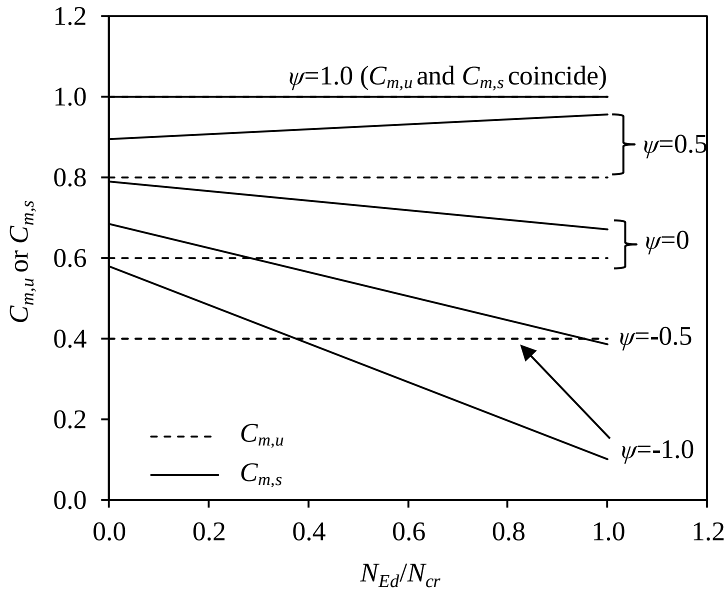

Fig. 16. Comparisons between $C_{m,u}$ and $C_{m,s}$ equivalent moment factors.

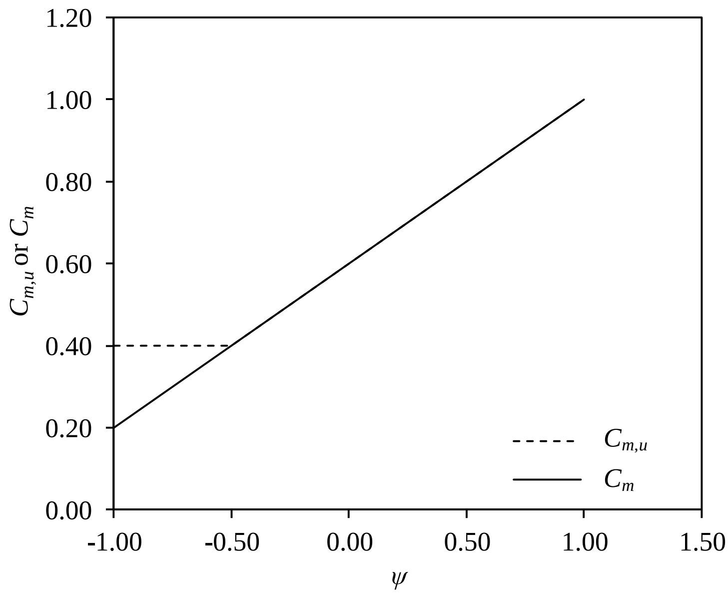

Fig. 17. Comparisons between equivalent uniform moment factors from American specification C_m and European code $C_{m,u}$.

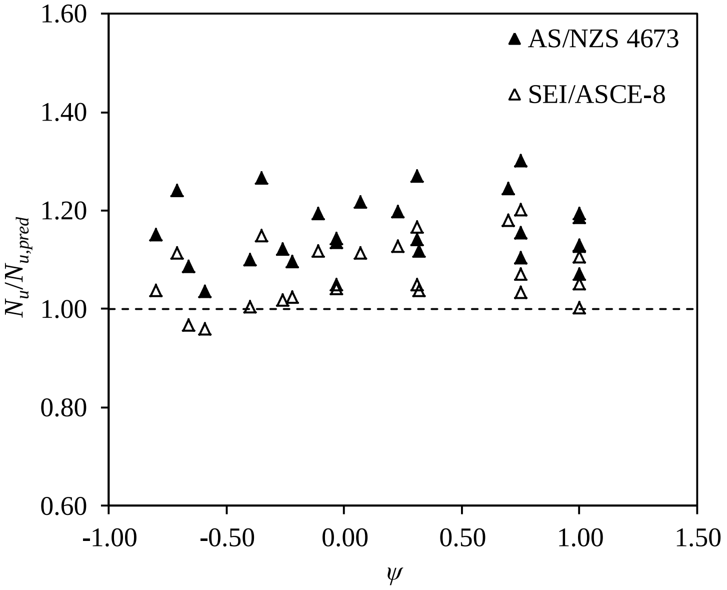

Fig. 18. Comparisons of test results with the AS/NZS 4673 and SEI/ASCE-8 strength predictions.

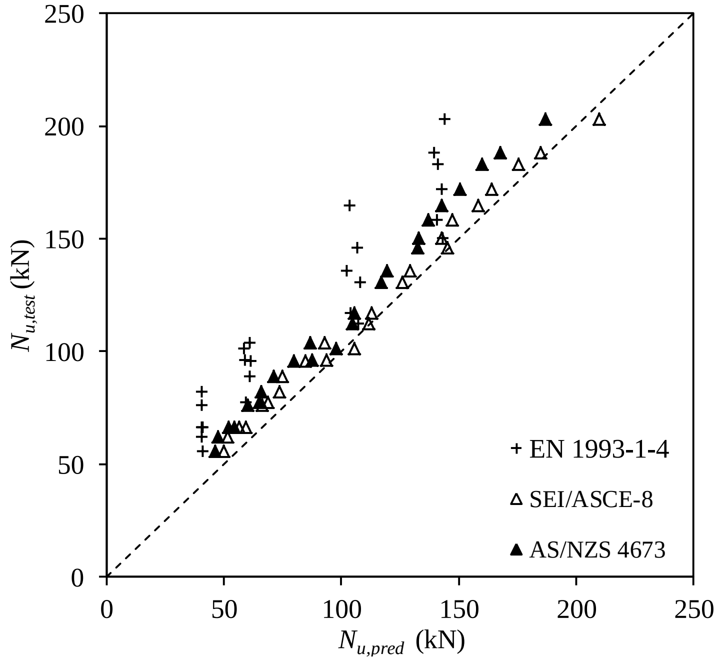

Fig. 19. Comparisons of test results with the codified strength predictions.

Table 1 Average measured tensile flat material properties.

Cross-section	E	$\sigma_{0.2}$	$\sigma_{1.0}$	σ_u	ε_u	ε_f	R-O coefficient		
	(GPa)	(MPa)	(MPa)	(MPa)	(%)	(%)	n	$n'_{0.2,u}$	$n'_{0.2,1.0}$
RHS 100×40×2	197	449	457	483	14.5	29.2	8.8	2.3	3.4
SHS 60×60×3	199	470	485	488	7.4	21.1	7.3	10.9	7.6

Table 2 Average measured tensile corner material properties.

Cross-section	E	$\sigma_{0.2}$	$\sigma_{1.0}$	σ_u	ε_u	ε_f	R-O coefficient		
	(GPa)	(MPa)	(MPa)	(MPa)	(%)	(%)	n	$n'_{0.2,u}$	$n'_{0.2,1.0}$
RHS 100×40×2	193	601	–	638	1.2	9.6	5.5	17.2	–
SHS 60×60×3	200	579	–	648	1.1	13.2	4.0	7.3	–

Table 3 Measured geometric dimensions and imperfections of the beam-column specimens.

Test series	Specimen	L (mm)	H (mm)	B (mm)	t (mm)	r_i (mm)	A (mm^2)	A_{eff} (mm^2)	ω_0 (mm)	ω_g (mm)
RHS 100×40×2-MI-500	1A	500.0	40.0	100.0	1.89	3.40	500.7	346.7	0.033	0.254
	1B	500.0	40.0	100.1	1.90	3.40	503.7	349.3	0.033	0.381
	1C	500.0	39.9	100.0	1.91	3.40	505.4	351.6	0.033	0.254
	1D	500.0	40.0	100.0	1.91	3.40	505.8	351.9	0.033	0.127
	1E	500.0	40.1	100.2	1.90	3.40	504.4	349.8	0.033	0.254
	1F	500.0	40.0	100.0	1.90	3.40	503.3	349.3	0.033	0.254
RHS 100×40×2-MI-1250	2A	1250.0	40.1	100.1	1.89	3.40	501.5	347.1	0.033	0.762
	2B	1250.0	40.0	100.0	1.90	3.40	503.3	349.3	0.033	0.508
	2C	1250.0	40.0	100.0	1.90	3.40	503.3	349.3	0.033	0.381
	2D	1250.0	40.0	100.0	1.90	3.40	503.3	349.3	0.033	0.508
	2E	1250.0	40.0	100.1	1.90	3.40	503.7	349.3	0.033	0.635
	2F	1250.0	40.3	100.0	1.89	3.40	501.8	347.8	0.033	0.635
SHS 60×60×3-600	3A	600.0	60.0	60.0	2.82	3.40	621.6	621.6	0.024	0.127
	3B	600.0	60.1	60.0	2.83	3.40	624.2	624.2	0.024	0.254
	3C	600.0	59.8	59.9	2.83	3.40	621.9	621.9	0.024	0.381
	3D	600.0	60.0	60.1	2.85	3.40	628.3	628.3	0.024	0.381
	3E	600.0	59.8	59.9	2.84	3.40	624.0	624.0	0.024	0.254
	3F	600.0	59.8	60.0	2.85	3.40	626.6	626.6	0.024	0.381
SHS 60×60×3-1200	4A	1200.0	60.1	60.1	2.83	3.40	624.8	624.8	0.024	0.508
	4B	1200.0	60.0	60.1	2.85	3.40	628.3	628.3	0.024	0.508
	4C	1200.0	59.8	60.0	2.83	3.40	622.5	622.5	0.024	0.635
	4D	1200.0	60.2	60.1	2.84	3.40	627.4	627.4	0.024	0.762
	4E	1200.0	59.8	60.2	2.85	3.40	627.8	627.8	0.024	0.635
	4F	1200.0	60.1	60.0	2.85	3.40	628.3	628.3	0.024	0.762

Note: MI indicates beam-column tests, in which bending was induced about the minor axis.

Table 4 Summary of beam-column test results.

Test series	Specimen	L_e (mm)	$\overline{\lambda}$	e_0 (mm)	ψ	N_u (kN)	$M_{u,b}$ (kNm)	$M_{u,t}$ (kNm)	$\phi_{u,b}$ (deg)	$\phi_{u,t}$ (deg)	$\delta_{u,L/2}$ (mm)	$\delta_{u,L/4}$ (mm)
RHS 100×40×2-MI-500	1A	674.8	0.52	20.6	-0.59	101.3	2.09	-1.23	0.84	0.13	1.53	1.75
	1B	674.8	0.52	20.6	-0.22	96.2	1.98	-0.44	1.04	0.43	2.38	2.43
	1C	674.8	0.52	19.6	-0.11	104.0	2.04	-0.22	1.08	0.52	2.61	2.68
	1D	674.8	0.52	19.5	0.23	95.9	1.87	0.43	1.19	0.82	3.40	3.22
	1E	674.8	0.52	19.6	0.70	88.7	1.74	1.22	1.32	1.20	4.43	3.94
	1F	674.8	0.52	20.3	1.00	77.6	1.58	1.58	1.44	1.44	5.26	4.37
RHS 100×40×2-MI-1250	2A	1424.8	1.09	19.8	-0.71	82.2	1.63	-1.16	2.27	0.72	10.80	10.67
	2B	1424.8	1.09	19.9	-0.35	76.2	1.52	-0.53	2.88	1.78	17.53	15.39
	2C	1424.8	1.09	20.0	0.07	66.5	1.33	0.09	3.24	2.51	21.47	18.07
	2D	1424.8	1.09	19.8	0.31	66.3	1.31	0.41	3.07	2.58	21.32	17.43
	2E[a]	1424.8	1.09	20.2	0.75	62.2	1.26	0.94	–	–	–	–
	2F	1424.8	1.08	19.7	1.00	55.5	1.09	1.09	3.10	3.10	23.39	18.25
SHS 60×60×3-600	3A	774.8	0.54	19.3	-0.66	203.0	3.92	-2.59	1.90	0.28	3.62	4.35
	3B	774.8	0.54	20.7	-0.26	188.3	3.90	-1.01	2.25	0.93	5.91	6.16
	3C	774.8	0.54	20.0	-0.03	182.9	3.66	-0.11	2.23	1.21	6.74	6.65
	3D	774.8	0.54	20.1	0.31	172.1	3.46	1.07	2.39	1.70	8.42	7.74
	3E	774.8	0.54	20.3	0.75	158.2	3.21	2.41	2.23	2.02	9.28	8.03
	3F	774.8	0.54	19.8	1.00	150.4	2.98	2.98	2.34	2.34	10.05	8.34
SHS 60×60×3-1200	4A	1374.8	0.95	20.6	-0.80	164.5	3.39	-2.71	2.37	0.59	10.30	10.87
	4B	1374.8	0.96	19.2	-0.40	146.1	2.81	-1.12	2.63	1.45	14.60	13.29
	4C	1374.8	0.96	20.6	-0.03	135.8	2.80	-0.08	2.92	2.09	18.26	15.65
	4D	1374.8	0.95	18.8	0.32	130.8	2.46	0.79	2.94	2.40	19.81	16.43
	4E	1374.8	0.96	20.3	0.75	116.9	2.37	1.78	2.98	2.76	21.38	16.72
	4F	1374.8	0.96	19.0	1.00	112.3	2.13	2.13	2.96	2.96	22.32	17.41

[a] No rotation and lateral deflection data were obtained due to a sudden electrical shutdown.

Table 5 Comparison of beam-column test results with predicted strengths.

Test series	Specimen	e_0	ψ	$N_u/N_{u,EC3}$	$N_u/N_{u,EC3\text{-}U}$	$N_u/N_{u,EC3\text{-}S}$	$N_u/N_{u,ASCE}$	$N_u/N_{u,AS/NZS}$
RHS 100×40×2-MI-500	1A	20.6	-0.59	1.72	1.08	1.32	0.96	1.03
	1B	20.6	-0.22	1.63	1.13	1.34	1.02	1.10
	1C	19.6	-0.11	1.70	1.24	1.44	1.12	1.19
	1D	19.5	0.23	1.55	1.26	1.40	1.13	1.20
	1E	19.6	0.70	1.45	1.34	1.41	1.18	1.24
	1F	20.3	1.00	1.30	1.30	1.32	1.13	1.19
RHS 100×40×2-MI-1250	2A	19.8	-0.71	2.01	1.42	1.53	1.11	1.24
	2B	19.9	-0.35	1.86	1.38	1.54	1.15	1.26
	2C	20.0	0.07	1.63	1.35	1.46	1.11	1.22
	2D	19.8	0.31	1.62	1.41	1.51	1.17	1.27
	2E	20.2	0.75	1.53	1.46	1.52	1.20	1.30
	2F	19.7	1.00	1.34	1.34	1.38	1.10	1.19
SHS 60×60×3-600	3A	19.3	-0.66	1.41	1.00	1.12	0.97	1.08
	3B	20.7	-0.26	1.35	1.00	1.14	1.02	1.12
	3C	20.0	-0.03	1.29	1.02	1.14	1.04	1.14
	3D	20.1	0.31	1.21	1.04	1.12	1.05	1.14
	3E	20.3	0.75	1.12	1.07	1.10	1.07	1.15
	3F	19.8	1.00	1.05	1.05	1.07	1.05	1.13
SHS 60×60×3-1200	4A	20.6	-0.80	1.59	1.17	1.22	1.04	1.15
	4B	19.2	-0.40	1.37	1.05	1.15	1.00	1.10
	4C	20.6	-0.03	1.32	1.09	1.18	1.05	1.14
	4D	18.8	0.32	1.21	1.08	1.14	1.04	1.12
	4E	20.3	0.75	1.12	1.08	1.12	1.03	1.10
	4F	19.0	1.00	1.04	1.04	1.07	1.00	1.07
	Mean			1.43	1.18	1.28	1.07	1.16
	COV			0.18	0.13	0.13	0.06	0.06